2022

Tidal current turbine blade optimisation with improved blade element momentum theory and a non-dominated sorting genetic algorithm

Eng Jet Yeo

David Kennedy

Fergal O'Rourke

Energy 250 (2022) 123720

Contents lists available at ScienceDirect

Energy

journal homepage: www.elsevier.com/locate/energy

Tidal current turbine blade optimisation with improved blade element momentum theory and a non-dominated sorting genetic algorithm

Eng Jet Yeo [a, *], David M. Kennedy [b], Fergal O'Rourke [c]

[a] Centre for Renewables and Energy, School of Engineering, Dundalk Institute of Technology, Dundalk, **CA**, Ireland
[b] Department of Mechanical Engineering, Technological University Dublin, Dublin, Ireland
[c] Centre for Renewables and Energy, School of Engineering, Dundalk Institute of Technology, Dundalk, Ireland

ARTICLE INFO

Article history:
Received 30 September 2021
Received in revised form
21 February 2022
Accepted 10 March 2022
Available online 19 March 2022

Keywords:
Tidal current turbine
Blade element momentum theory
XFoil
Genetic algorithm
Optimisation

ABSTRACT

Tidal current energy has the advantage of predictability over most of the other renewable energy resources. However, due to the harsh operating environment and complicated site conditions, developments in this domain have been gradual. Paramount to these points is device design and optimisation of hydrodynamic performance. Recent developments in the correction models of BEM theory have further improved the accuracy of the prediction model. Using an improved blade element momentum theory model that is capable of accurately capturing the downwash angle and combining it with a well-developed and reliable non-dominated sorting genetic algorithm model, an effective and efficient tidal current turbine blade optimisation tool has been developed and is presented in this paper. This novel work incorporated a NACA generator that is capable of reproducing any NACA profile, such a tool allows the solver to analyse each and every profile used in each spanwise blade element. As a result, the model is very effective at producing tidal current turbine blades that have been optimised not only for local twist angle and chord length, but also for the suitable NACA profiles to be used at a particular spanwise blade element. The use of the non-dominated sorting genetic algorithm in this work allows the model to efficiently explore a wide range of solutions, outputting a number of tidal current turbine blades suitable for a specified operating condition. The accuracy of the performance prediction of the improved BEM model is validated against an experimentally validated tidal current turbine blade. The coefficient of determination (R^2) values for power and thrust coefficient are 0.99828 and 0.99488 respectively when comparing this work with experimental measurements found in the literature. Furthermore this proves that the improved BEM model is capable of efficiently predicting hydrodynamic performance of a tidal current turbine blade to a high degree of accuracy. Further work includes implementing computational fluid dynamics for further validation and evaluation.

Credit author statement

Eng Jet Yeo: Conceptualization, Methodology, Software, Validation, Writing – original draft. David M. Kennedy: Supervision. Fergal O'Rourke: Writing – review & editing, Supervision

1. Introduction

Recently there has been an increase in the number of companies pursuing tidal current energy, using tidal current turbines (TCT), to tap into the relatively large unexploited tidal energy. Furthermore, some of the prototypes and projects have demonstrated successful commercialisation. One of such examples is Verdant Power's TCT, the company's grid-connected tidal power has exceeded performance projections by 40%, generating over 275 MWh over eight months of continued operation [1]. Another example is Magallanes Renovables, the company has successfully reinstalled their second generation 2 MW tidal platform 'ATIR' in April 2021 and connected to the national grid in the Fall of Warness in Orkney, Scotland [2]. The AR500 from SIMEC Atlantic Energy, installed in Naru Island, Japan, has made a recent milestone, the device has successfully passed one of the strongest tides of the year, followed by exhaustive inspection and verification of all the involved equipment. The device has also outputted more than 90 MWh of energy since the

* Corresponding author.
E-mail addresses: engjet.yeo@dkit.ie (E.J. Yeo), david.kennedy@tudublin.ie (D.M. Kennedy), fergal.orourke@dkit.ie (F. O'Rourke).

https://doi.org/10.1016/j.energy.2022.123720

Nomenclature

Greek

α	Angle of attack
α_i	Effective angle of attack
γ	Blade twist angle
λ_r	Local tip speed ratio
ν	Kinematic viscosity of fluid
φ	Angle of relative fluid
ρ	Density of fluid
σ	Local blade solidity

Roman

$\bar{c}$	Geometric mean chord length
a	Axial induction factor
a'	Angular induction factor
a_c	Critical axial induction factor
B	Number of blades
C	Chord length
C_D	Drag coefficient
C_L	Lift coefficient
C_n	Normal force coefficient
C_P	Power coefficient
C_t	Tangential force coefficient
C_T	Thrust coefficient
$C_{D,e}$	Drag coefficient at effective angle of attack
$C_{L,2D}(\alpha)$	2D hydrofoil's lift coefficient at local angle of attack
$C_{L,e}$	Lift coefficient at angle of attack
CD	Crowding distance
D	Diameter of the rotor
dF_D	Drag force
$\boldsymbol{dF_L}$	Lift force
dF_N	Normal force
dF_{tan}	Tangential Force
dT	Local Thrust
dr	Blade element thickness
F	Resultant loss correction factor
F_1	Shen's correction constant F1
f_1	Objective function 1
f_2	Objective function 2
f_3	Objective function 3
F_n	Normalised fitness value
F_R	Three-dimensional downwash factor
F_S	Rotational factor
F_{hub}	Hub loss correction factor
F_{tip}	Tip loss correction factor
F_{total}	Sum of fitness values
g_1	Coefficient constant for Shen's correction model
m	Curve slope of the linear zone of hydrofoil lift profile
M_B	Fap-wise bending moment
n	Pareto front number
P_C	Crossover probability
P_M	Mutation probability
R	Radius of the rotor
R_{hub}	Radius of the rotor hub
r	Local radial position on the blade
Re	Reynolds number
S	Blade area between local radial position and the blade tip
U	Free stream velocity
Y_1	Shen's correction constant Y1
Y_2	Shen's correction constant Y2

List of abbreviations

BEM	Blade element momentum
CFD	Computational fluid dynamics
GA	Genetic algorithm
MAE	Mean absolute error
NSGA	Non-dominated sorting genetic algorithm
RMSE	Root mean squared error
TCT	Tidal current turbine
TSR	Tip speed ratio

installation in January 2021 [3]. Despite the success of tidal energy devices for a number of companies, the tidal energy sector is still some way behind other mature renewable energy technologies, such as wind energy and this is evident in the large body of literature investigating the effects of different tidal current turbine designs under various operating conditions experienced at real tidal current energy sites [4–9]. Optimisation of tidal current turbines plays a major role in improving the performance, life span and the economics. This is paramount to ensure full commercialisation of tidal current energy systems.

The work presented in this paper focuses on a coupled multi-objective non-dominated sorting genetic algorithm (NSGA) and blade element momentum (BEM) theory. The BEM theory has been widely utilised in the wind industry and has proved to be one the most common and computationally efficient methods to predict the aerodynamic/hydrodynamic performance acting on the blades of wind turbines as well as TCTs [10–15]. Vogel et al. [16] have comprehensively described the main difference between TCTs and wind turbines is the volume flux constrained flow field that occurs around TCTs. The authors have further extended the BEM theory to take into account the effects of flow confinement for the case of TCTs. Masters et al. [17] have presented a BEM model with the inclusion of Prandtl's correction model and have validated against the lifting line theory model and an industrial code, GH Tidal Bladed, the presented results have shown good correlations with the code. El-shahat et al. [18] found that the results of BEM theory were in good agreement with experimental data presented by Bahaj et al. [19] at low values of Ncrit parameter (Ncrit value is used to measure the free flow turbulence and to simulate the turbulent transition location in XFoil) when using the XFoil code for lift and drag coefficients. Using the same experimental data, the study undertaken by El-shahat et al. has also shown better thrust coefficient prediction and a more realistic power coefficient prediction over a range of tip speed ratios in their BEM model when compared to the SERG-Tidal model by Bahaj et al. [19].

In addition to the BEM theory, the use of genetic algorithm (GA) has also been widely used as an optimisation tool in the wind industry and proven to save computational time. Early studies undertaken by Selig and Coverston-Caroll [20] have demonstrated the use of GA in wind turbine design to maximise the annual energy output by optimising the blade pitch, chord and twist distribution. Sessarego et al. [21] have used NSGA to optimise annual energy output and optimising the flap-wise bending moment of the wind turbine. There are many other studies done using GA in an attempt to further improve the performance of wind turbines and wind farm layout [22–31]. As tidal current turbines share a number of similarities with wind turbines, a GA model can be similarly implemented to optimise a TCT blade. Sale [32] has used the

coupled GA and BEM to optimise a TCT for an ideal power curve while avoiding cavitation inception. Kolekar and Banerjee [33] have used GA to improve power coefficient and reduced flap-wise bending stress by optimising pitch angles, tip speed ratios (TSR) and chord length, and it was further validated using CFD. Zhu et al. [34] have demonstrated the use of neural networks and GA to optimise a TCT blade and has shown improvement in power coefficient as well as for an expanded range of optimal tip speed ratios, the optimised TCT blade has been further validated against an experiment in a cavitation tunnel as well as sea trials on Xiushan island, Zhejiang province, China. Menéndez et al. [35] have used the surrogate-based optimisation method to replace the computationally expensive computational fluid dynamics (CFD) simulation in predicting the hydrodynamic performance of a TCT blade and utilised multi-objective GA to find the optimum blade geometry, the output blades as a result have shown improvement in terms of hydrodynamic performance when compared to their base case. There are many more studies presented in the literature proving that effectiveness and efficiency of using GA in terms of optimising TCT designs [36–42].

The work presented in this paper is an optimisation tool for TCT blades using combined NSGA and an improved BEM model along with a NACA generator. Using an improved BEM model that accurately captures the downwash angle, a well-developed and reliable NSGA has also been used to improve the optimisation efficiency, resulting in a solver with higher fidelity. On top of that, the optimisation tool in this work incorporated a NACA generator that is capable of reproducing any NACA profile, such a tool allows the solver to analyse each and every profile used in each spanwise blade element. As a result, the model is very effective at producing tidal current turbine blades that have been optimised not only for local twist angle and chord length, but also for suitable NACA profiles to be used at a particular spanwise blade element. Additionally, this model also allows further implementation of other hydrofoil profiles that can be similarly generated using other approaches, expanding the capability to explore more hydrofoil profiles to be considered in the optimisation process. A set of Pareto optimal solutions have been produced in this work and each solution represents a completely unique tidal current turbine blade profile. Whereas other studies in the literature have used GA to only determine new hydrofoil profiles, optimising for the resulting lift and drag, and then used these results as model inputs into a BEM solver. The model used in this work focuses on maximising the power coefficient across a range of tip speed ratios while reducing the overall flap-wise bending moment by optimising for NACA profiles, twist angle and chord length at each blade element along the span of the tidal current turbine blade.

2. Theory

In this section, an improved blade element momentum (BEM) theory model is described, followed by a description of XFoil in terms of accuracy and the non-dominated sorting genetic algorithm (NSGA) employed in this work.

2.1. Blade element momentum theory

In a classic blade element momentum (BEM) theory, a few assumptions are made. The one-dimensional momentum theory assumes that the flow perpendicular to the rotor disc is steady, homogenous and incompressible. The rotor is assumed to have an infinite number of blades and no frictional drag between the turbine and the fluid. The static pressure of the fluid far upstream is equal to the static pressure of the fluid far downstream. For blade element theory the blade is divided into a number of spanwise blade elements, where each of the elements experience different fluid flow conditions due rotational velocity and the local element geometry such as hydrofoil profile, chord length, and twist angle.

As previously described in another paper by the authors [43], the hydrodynamic parameters on each blade element are illustrated in Fig. 1. The angles in Fig. 1 consist of angle of attack, α, and relative angle of the tidal current flow, φ. Fig. 1 also includes the tangential force, dF_{tan}, lift force, dF_L, normal force, $dF_{N,}$ and drag force, dF_D. The horizontal broken line in Fig. 1 represents the rotor plane.

The BEM theory initially uses an assumption of an infinite number of turbine blades, which is not realistic and has to be corrected. To improve the accuracy of the BEM, tip loss correction factor is employed. There are several tip loss correction models proposed in the literature such as Glauert's characteristic equation [44], Wilson et al. [45,46], Goldstein [47] and Shen's correction [48]. The correction model used in this research is a validated and improved model based on Shen's correction model by Zhong et al. [49]. The authors introduced two factors to the model, one is the downwash due to the three-dimensional effect, F_S, and the other is due to the rotational effect, F_R, as described in Equations (1) and (2).

$$F_R = 2 - \frac{2}{pi}\cos^{-1}\left\{\exp\left[-2B\left(1-\frac{r}{R}\right)\sqrt{1-\lambda_r^2}\right]\right\} \tag{1}$$

$$F_S = \frac{2}{pi}\cos^{-1}\left\{\exp\left[-\left(\frac{R-r}{\bar{c}}\right)^{\frac{3}{4}}\right]\right\} \tag{2}$$

where B is the number of blades, R is the radius of the turbine, r is the radial position of the blade element, λ_r is the local tip speed ratio and $\bar{c}$ is the geometric mean chord length,

$$\bar{c} = \frac{S}{R-r} \tag{3}$$

where S is the blade area between the local radial position and the blade tip. In addition to the two new factors introduced by Zhong et al. Prandtl's tip loss correction factor [10], F_{tip}, is used and is described in Equation (4).

$$F_{tip} = \frac{2}{\pi}\cos^{-1}\left[\exp\left(\frac{B(R-r)}{2r\sin\varphi}\right)\right] \tag{4}$$

Similarly, the hub loss model, F_{hub}, is employed to correct the induced velocity as a result of vortex shedding near the hub of the rotor.

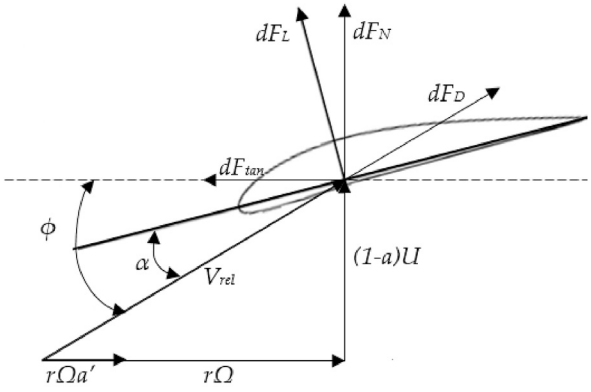

Fig. 1. Section blade element diagram of a tidal current turbine showing angles, forces and velocities.

$$F_{hub} = \frac{2}{\pi}\cos^{-1}\left[\exp\left(\frac{B(r - R_{hub})}{2r\sin\varphi}\right)\right] \tag{5}$$

where R_{hub} radius of the rotor hub. The tip and hub losses can be multiplied to get the resulting losses, $F = F_{hub}F_{tip}$. As Zhong et al. described in his study, the lift and drag coefficients, C_L and C_D of the local blade element have to be corrected.

$$C_L = \frac{1}{\cos^2\alpha_i}\left(C_{L,e}\cos\alpha_i - C_{D,e}\sin\alpha_i\right) \tag{6}$$

$$C_D = \frac{1}{\cos^2\alpha_i}\left(C_{D,e}\cos\alpha_i + C_{L,e}\sin\alpha_i\right) \tag{7}$$

where α_i is the downwash angle which is determined using Equation (8), $C_{L,e}$ and $C_{D,e}$ are the 2D hydrofoil's lift and drag coefficient at effective angle of attack, α_e.

$$\alpha_i = \frac{C_{L,2D}(\alpha)}{m}(1 - F_S) \tag{8}$$

where $C_{L,2D}(\alpha)$ is the 2D hydrofoil's lift coefficient at the local angle of attack, α, and m is the curve slope of the linear zone of the hydrofoil lift coefficient profile before the stall angle. The axial induction factor, a, and the angular induction factor, a', can then be calculated as shown in Equations (9) and (10).

$$a = \frac{2 + Y_1 - \sqrt{4Y_1(1 - F_R) + Y_1^2}}{2(1 + F_R Y_1)} \tag{9}$$

$$a' = \frac{1}{\frac{(1 - aF_R)Y_2}{1 - a} - 1} \tag{10}$$

where

$$Y_1 = \frac{4F_R\sin^2\varphi}{\sigma C_n F_1} \tag{11}$$

$$Y_2 = \frac{4F_R\sin\varphi\cos\varphi}{\sigma C_t F_1} \tag{12}$$

$$F_1 = \frac{2}{\pi}\cos^{-1}\left[\exp\left(-g_1\frac{B(R - r)}{2r\sin\varphi}\right)\right] \tag{13}$$

$$g_1 = \exp[-0.125(B\lambda - 21)] + 0.1 \tag{14}$$

where σ is the local solidity defined by $\sigma = \frac{CB}{2\pi r}$ where C is the chord length and B is the number of blades. The normal force coefficient, C_n, and tangential force coefficient, C_t, are calculated as follows.

$$C_n = C_L\cos\varphi + C_D\sin\varphi \tag{15}$$

$$C_t = C_L\sin\varphi - C_D\cos\varphi \tag{16}$$

When the axial induction factor, a becomes larger than the critical value, $a_c = 1/3$, the momentum theory is no longer valid and Glauert's correction is employed to calculate the local thrust coefficient, C_T. This work uses a modified Glauert's correction by Shen et al. [48] which is compatible with the current improved BEM algorithm.

$$C_T = \begin{cases} 4aF(1 - aF), & a < a_c \\ 4\left[a_c^2F^2 + (1 - 2a_cF)aF\right], & a \geq a_c \end{cases} \tag{17}$$

The flapwise bending moment of the blade can be calculated with Equation (18), based on the assumption that the turbine blade is modelled as a cantilever beam supported at the blade root [50].

$$M_B = \frac{1}{B}\int_0^R rdT \tag{18}$$

where

$$dT = \frac{1}{2}\rho\pi C_T U^2 2rdr \tag{19}$$

and ρ is the density of seawater and dr is the blade element thickness.

2.2. Reynolds number and XFoil

XFoil is code that is used in the current study to analyse the lift and drag coefficients of the generated NACA hydrofoil profiles. As the lift and drag characteristics are the fundamental in accurately determining the axial and tangential forces on each blade element, the reliability of XFoil is paramount. Xfoil has been widely studied in the literature. Van Treuren [51] has performed experimental tests of wind turbine airfoils and have stated that the XFoil code is not robust enough for predicting the aerodynamic performance at low Reynolds number (below Re = 100,000). Similarly, Mack et al. [52] performed an analysis on a modified NACA 64_3−618 profile at low Reynolds numbers (Re = 64,200 and Re = 137,000) and have concluded that XFoil is not capable of capturing the effects of separated laminar boundary layer and the formation of a closed laminar separation bubble, leading to inaccuracy of results produced by XFoil.

On the contrary, Van Treuren [51] have stated that the simulation results generated by XFoil are generally adequate at Reynolds number greater than 500,000 as the flow will stay attached to the airfoil. Timmer and Bak [53] have discussed and shown that XFoil and its extension RFoil have produced results with good agreement with measured data at Re = 6,000,000. Zhu et al. [54] have designed new airfoil profiles optimised for Re = 16 million using XFoil and the results are in good agreement with a CFD solver. Pires et al. [55] have conducted tests on the DU00W212 airfoil at high Reynolds numbers of 3, 6, 9, 12 and 15 million at the DNW high pressure wind tunnel in Göttingen. It was confirmed that as Reynolds numbers increase, the minimum drag decreases and maximum lift increases. There is negligible change in lift coefficients in the linear region (angle of attack between −7° to 10°) at different tested Reynolds numbers. The test results have provided invaluable insights on the airfoil aerodynamic behaviour at high Reynolds numbers. Pires et al. have also performed tests of high Reynolds numbers (Re = 3,000,000 and Re = 6,000,000) at the wind tunnel of LM Wind Power. In the same article, the authors have compared the measured data with XFoil, It was shown that XFoil is capable of predicting results of good agreement by fine tuning the N-factor and Mach number [56]. A study conducted by Selig [57] has proven that XFoil is well suited for analysis of airfoils at Reynolds numbers (between Re = 100,000 and Re = 500,000). It was agreed by Morgado et al. [58] showing that XFoil remains an excellent airfoil design and analysis tool, providing sufficient accuracy at the phase of conceptual designs.

Similar to Ouro et al. [59], the Reynolds numbers for the current

work is based on the turbine rotor's diameter, described in Equation (20).

$$Re_D = \frac{UD}{\nu} \tag{20}$$

where U is the velocity of the fluid, D is the diameter of the rotor, and ν is the kinematic viscosity of the fluid.

2.3. Non-dominated sorting genetic algorithm

The genetic algorithms (GA) are part of evolutionary computation models that are capable of effectively and efficiently optimising problems with the process of biologically inspired operators such as natural selection, crossover and mutation. In nature, the natural selection ensures that individuals that are fitter than others are more likely to survive and produce offspring. The natural selection is a mechanism that assigns probabilities to the individuals, individuals with a higher fitness value are more likely to be selected and therefore contribute more to the production of the next generation. These probabilistic search procedures are designed to work on large data sets that can be represented by strings [60]. Each string can also be imagined as strands of chromosomes and in each chromosome, there are genes.

In this work, with the blade element moment (BEM) model, the tidal current turbine blades were split into multiple blade elements to determine the local hydrodynamic performance. By specifying the operating condition and local blade element profile such as NACA profile, twist angle, and chord length, the BEM model outputs the local power and thrust coefficient as a result. The genes in the current GA model are represented by the local blade element profile, and the chromosomes can then be represented with tidal current turbine blades.

There are four phases in the GA, namely Selection, Crossover, Mutation, and Repopulation. The selection will select pairs of blades based on their fitness value, a higher fitness value results in a higher chance of being selected to proceed in the next phase. The fitness functions employed in the current study are power coefficient at design tip speed ratio (TSR), f_1, mean power coefficient at plus and minus two steps of design TSR, f_2, and the mean overall bending moment of the tidal current turbines across the range of TSR, f_3. The fitness functions f_1, f_2, and f_3 are described as follows:

$$f_1 = C_{P,i} \tag{21}$$

$$f_2 = \frac{\sum_{i-2}^{i+2} C_{P,i}}{5} \tag{22}$$

$$f_3 = \frac{\sum M_B}{TSR_n} \tag{23}$$

where i is the designed TSR and M_B is the bending moment of the blade.

The blades are selected with the proportional roulette wheel function described in Equation (24), where F_ν is the fitness value of the blade, F_{total} is the sum of fitness values of the current population and F_n is the normalised fitness value of the tidal current turbine blade.

$$F_n = \frac{F_\nu}{F_{total}} \tag{24}$$

The proportional roulette wheel selection allows all the individuals to be selected, the selection chance of each individual is directly proportional to their fitness value. Therefore, individuals with high fitness values are selected with greater likelihood than individuals with low fitness values.

Once a pair of blades are selected, they will undergo crossover or known as recombination, exchanging local blade element profiles such as the hydrofoil profile, twist angle and/or chord length, depending on the specified crossover probability, P_C, inheriting the characteristics of both parent blade parameters, producing a pair of potentially better performing tidal current turbine blades in the next generation. The crossover of parameters will only happen between the blade section of the same radial position, for example, sections towards blade root will not be cross-overed with sections towards the blade tip.

Schimitt L.M [50]. discussed that mutation plays a key part in the random generator phase of the GA. If the crossover operation combined with fitness selection without mutation, the convergence effect for the algorithm will exhibit genetic drift, which is a phenomenon when the populations become genetically identical. The mutation mechanism randomly mutates a few of the genes of the post-crossover chromosomes, this allows the GA to explore solutions beyond the initial population. In the current work, mutation randomly occurs after the cross-over operation depending on the mutation probability, P_M, to prevent pre-mature convergence and exploring solutions beyond the initial population set. The mutation may occur to change the local NACA profiles, randomly increase or decrease the twist angle and/or chord length, provide offspring blades with a wider variety of local blade element profiles. As a boundary condition set for the current study, each section is allowed to have up to a 10% change in parameter when mutation occurs to avoid drastic changes. The mutation and crossover theory is comprehensively detailed by Schimitt L. M [61].

The last phase of the GA model in the current study is done by the non-dominated sorting method, hence non-dominated sorting genetic algorithm (NSGA). Each blade is evaluated to determine if the blade is dominated by others in the current population, all non-dominated tidal current turbine (TCT) blades are the Pareto optimal solution, or known as the Pareto Frontier in the current population. For example, in a case of two objective functions, f_1 and f_2, if any chromosome is not dominated by any other chromosomes in terms of f_1 and f_2, the non-dominated chromosomes are considered as the Pareto Front 1. Once a frontier has been determined, the sorting process will repeat for the entire population to search for Pareto Front 2, 3, 4 and so on. The TCT blades are sorted using the crowding distance method as described in Equations (25) to (26)

$$CD_{i,n_{f_1}} = \frac{F_n(f_{1i+1}) - F_n(f_{1_{i-1}})}{F_n(f_{1max}) - F_n(f_{1min})} \tag{25}$$

$$CD_{i,n_{f_2}} = \frac{F_n(f_{2i+1}) - F_n(f_{2_{i-1}})}{F_n(f_{2max}) - F_n(f_{2min})} \tag{26}$$

$$CD_{i,n_{f_3}} = \frac{F_n(f_{3i+1}) - F_n(f_{3_{i-1}})}{F_n(f_{3max}) - F_n(f_{3min})} \tag{27}$$

$$CD_i = CD_{i,n_{f_1}} + CD_{i,n_{f_2}} + CD_{i,n_{f_3}} \tag{28}$$

for $i = 2, \ldots, (l-1)$,

Where l is the total number of chromosomes in the Pareto Front Number, n, and f_1, f_2 and f_3 are objective function 1, 2 and 3 respectively. The crowding distance, CD for $i = 2$ and $i = l$ is infinity. Once the CD is determined for the entire population, the TCT blades are sorted by CD in descending order. This mechanism ensures that TCT blades in the smallest Pareto Front Number will be selected for reservation in the next generation, then, TCT blades with furthest

distance apart from each other in the same Pareto Front Number are prioritised to be reserved to the next generation. A detailed description of the Non-dominated Sorting theory used in NSGA-II can be found in Refs. [21,39,62,63].

3. Methodology

The coupled non-dominated sorting genetic algorithm – blade element momentum (NSGA-BEM) model begins by randomly generating tidal current turbine blades in the initial population, using the experimentally validated 63-8xx Series tidal current turbine blade [19,64] as a sample. A variety of NACA profiles are generated using the NACA Airfoil generator [65] and the lift and drag characteristic of each NACA profile are predicted using XFoil and stored in a virtual growing library, which allows the ease of access for the optimisation model, saving computational time. The integrated NSGA-BEM model is then let to run according to the parameters tabulated in Table 1.

The optimisation process of the NSGA-BEM is illustrated in Fig. 2. After the initial population, all tidal current turbine (TCT) blades will go through BEM prediction and sorted before the NSGA sequence begins to iterate until the set number of generations is achieved. At the end of each generation, each TCT blade that has undergone crossover or mutation will go through the BEM prediction again to re-evaluate the new hydrodynamic performance. At the end of each generation, the population size will double the initial set amount, the TCT blades are sorted and any excess TCT blades beyond the population limit are eliminated from the current population pool. It is important to note that all TCT blades generated are stored as a different variable which can be used for data processing at the end of the sequence.

4. Results and discussion

The coupled non-dominated sorting genetic algorithm – blade element momentum (NSGA-BEM) tool was let to run for 300 generations, 100 blade profiles in each generation and it took approximately 16 hours to complete on an Intel® Core™ i7-8750H CPU, producing a total of 30,000 blade profiles. Full details on the model outputs and results are given in subsections below.

4.1. Validation of the current BEM solver

The accuracy of the improved blade element momentum (BEM) model was first validated against an experimentally validated tidal turbine blade profile, the NACA 63-8xx series by Bahaj et al. [19,64]. Fig. 3(a) and 4(a) show the predicted power coefficient with measured data against tip speed ratio. There is only slight variation of the prediction of power coefficient over the range of tip speed ratios when compared with the measured data and there is a minor underprediction of thrust coefficient across the range of tip speed ratios (TSR) using the improved BEM model. The improved BEM model demonstrates competency at predicting the hydrodynamic forces acting on the tidal current turbine blade with a high degree of accuracy when compared to basic BEM model with Glauert's correction as shown in Fig. 3(a) and 4(a). When the measured data is plotted against the predicted results as shown in Fig. 3(b) and 4(b), a diagonal straight line is presented, the mean absolute error (MAE), coefficient of determination (R^2) and root mean squared error (RMSE) are determined. It can be seen that MAE, R^2, and RMSE of power coefficient are 0.01761, 0.99828 and 0.020317 respectively with a minor overestimation on average when comparing the predicted against measured values. In terms of thrust coefficient, the MAE, R^2, and RMSE were found to be 0.021971, 0.99488 and 0.025816 respectively with minor underestimation overall.

Table 1
Parameters of the NSGA-BEM model.

Parameters	Value
Maximum number of generations	300
Population size	100
Crossover probability, P_C	0.8
Mutation probability, P_M	0.2
Design tip speed ratio	6

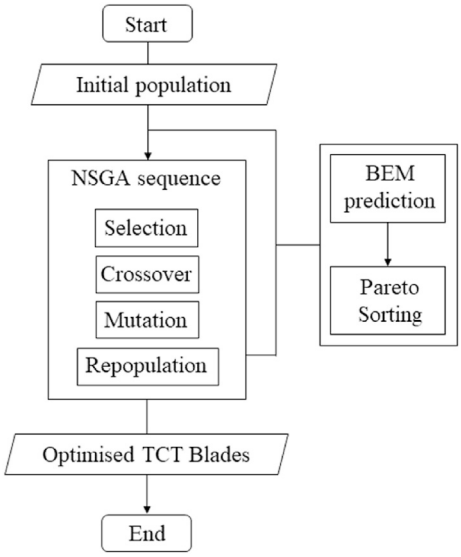

Fig. 2. The coupled non-dominated sorting genetic algorithm – blade element momentum theory optimisation process.

4.2. Pareto solutions

The coupled non-dominated sorting genetic algorithm – blade element momentum (NSGA-BEM) model has almost consistently generated 100 new turbine blade profiles in each generation, depending on a number of factors, such as the crossover probability, P_C, mutation probability, P_M, and selection probability of blades in the previous generation depending on the fitness function. Fig. 5 shows a 3-D plot of the three objective functions, where f_1, f_2, and f_3 are in the x, y, and z axis of the plot respectively and as defined in Equation (21) – (23). Fig. 6(a) and Fig. 6(b) are the 2-D plots of the Pareto solution with f_1 versus f_2 and f_2 versus f_3. In Fig. 5 and 6, each of the generated tidal current turbine blade profiles are represented with dots, it can be seen that the sample blade, 63-8xx series is grouped in the dominated solutions as it was one of the sample blades in the first generation. The current model then attempted to search for better solutions for the set objective functions, resulting in 248 blade profiles in the Pareto frontier out of 30,000 blade profiles. The selection of the solution was undertaken manually, Solution 1 was selected with the highest f_1 value, Solution 2 was selected for minimum f_3 value while having the f_1 value higher than 0.47, and finally, Solution 3 was selected between the two extremes.

4.3. Optimised blades

The three selected blades all have slight variations to at each blade element and are tabulated in Tables 2–4. The blade profiles are also illustrated in Figs. 7–9 and Selected Solution 1, 2 and 3

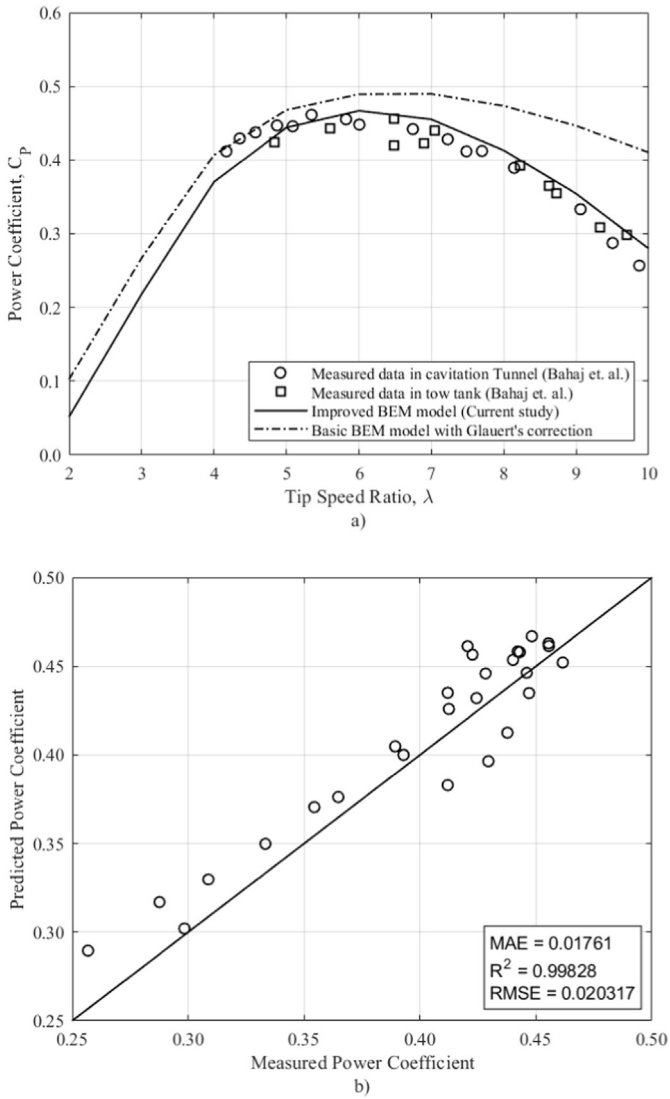

Fig. 3. (a) Comparison of predicted power coefficients and measured data versus tip speed ratio for the NACA 63-8xx Series tidal current turbine blade [19,64] and (b) Predicted power coefficients versus measured power coefficients of 63-8xx Series tidal current turbine blade.

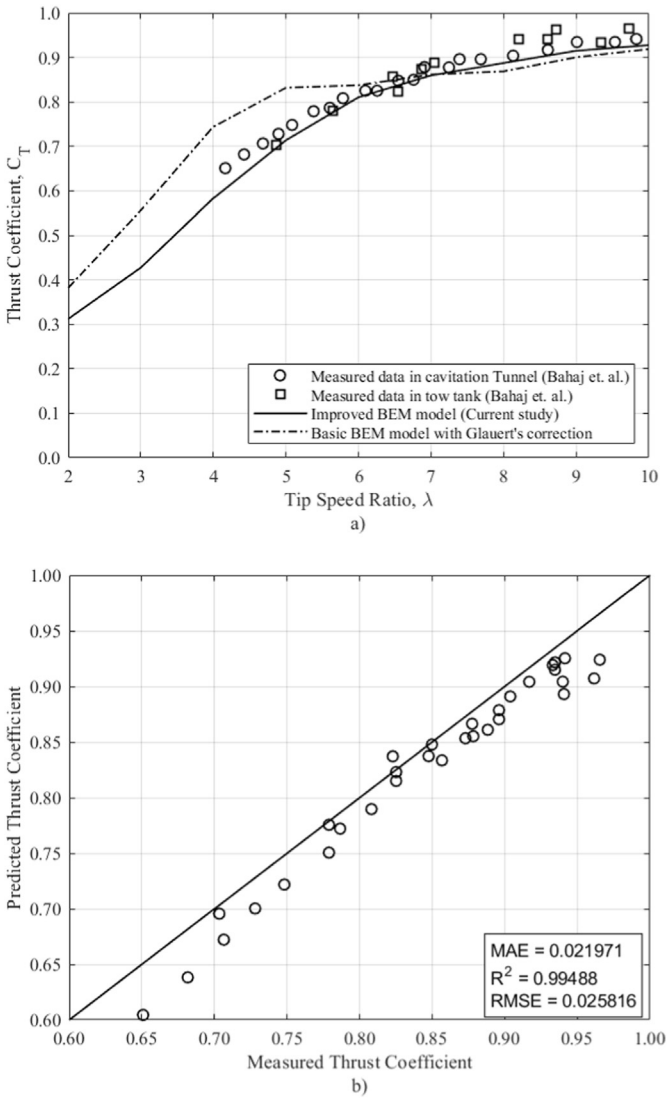

Fig. 4. (a) Comparison of predicted thrust coefficients and measured data versus tip speed ratio for the NACA 63-8xx Series tidal current turbine blade [19,64], and (b) Predicted thrust coefficients versus measured thrust coefficients of 63-8xx Series tidal current turbine blade.

respectively. It is observed that all three selected solutions output contain the same NACA profile which is the 6415 from radial position between 0.5 and 0.8, the last two sections of Solution 2 and 3 also output the same NACA profile, NACA 661413/2. These two NACA profiles are plotted in Fig. 10 to show and compare the lift and drag coefficients.

4.4. Performance comparison

The hydrodynamic performances for the selected solutions are plotted to compare with the sample blade as shown in Fig. 11 and Fig. 12. As shown in the figures, Selected Solution 1 outperforms the sample blade at a range of tip speed ratios (TSR) around a value of TSR = 5 and has a lower thrust coefficient for values lower than a TSR = 7, which is within the range of the specified designed TSR for the current study. Solution 2 and 3 showed similar performance characteristics, in terms of power and thrust coefficients, both solutions only outperform the sample blade at a TSR = 6 and above and slightly have an improved performance when compared to

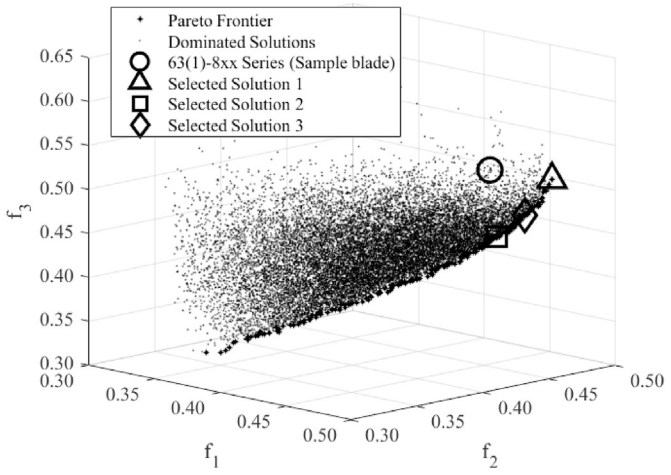

Fig. 5. 3-D plot of the Pareto solutions, each dot represents a tidal turbine blade profile.

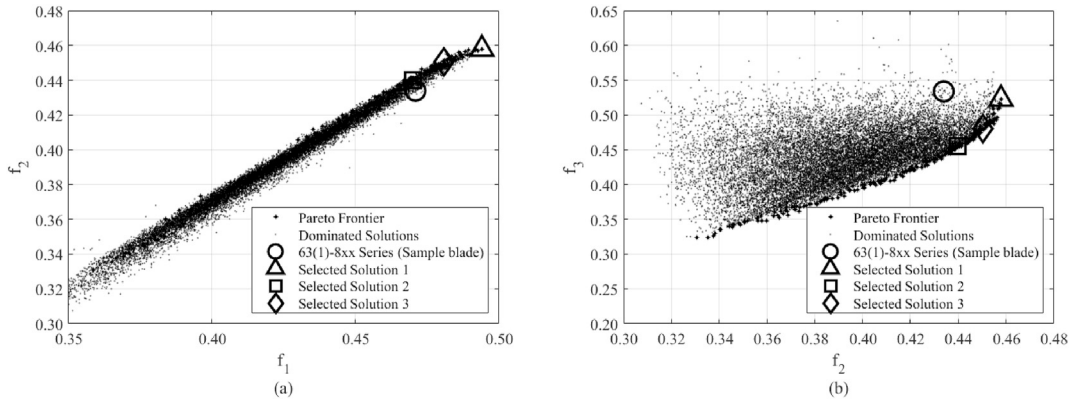

Fig. 6. 2-D plot of the Pareto solutions, (a) f_1 versus f_2 and (b) f_2 versus f_3.

Table 2
Blade profile of Selected Solution 1.

r	0.2	0.3	0.4	0.5	0.6	0.7	0.8	0.9	1.0
NACA	4421	651,820	632,818	6415	6415	6415	6415	654,613	654,612
C/R	0.1560	0.1134	0.1025	0.0870	0.0741	0.0646	0.0576	0.0554	0.0532
γ (°)	21.42	15.23	11.3	8.69	8.46	5.68	5.96	4.99	4.02

Table 3
Blade profile of Selected Solution 2.

r	0.2	0.3	0.4	0.5	0.6	0.7	0.8	0.9	1.0
NACA	4523	24,021	654,619	6415	6415	6415	6415	661,413	661,412
C/R	0.1325	0.1230	0.0965	0.1002	0.0667	0.0614	0.0489	0.0517	0.0545
γ (°)	25.19	14.74	14.15	10.66	8.14	7.45	6.05	5.17	4.29

Table 4
Blade profile of Selected Solution 3.

r	0.2	0.3	0.4	0.5	0.6	0.7	0.8	0.9	1.0
NACA	23,022	24,020	634,819	6415	6415	6415	6415	661,413	661,412
C/R	0.1325	0.1350	0.1051	0.0996	0.0737	0.0652	0.0602	0.0517	0.0432
γ (°)	23.93	15.67	12.65	10.25	8.62	7.62	6.24	5.17	4.10

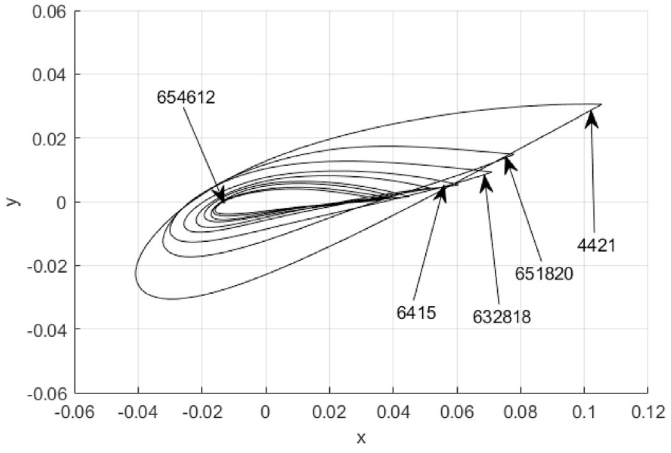

Fig. 7. 2-D section view of blade profile of Selected Solution 1.

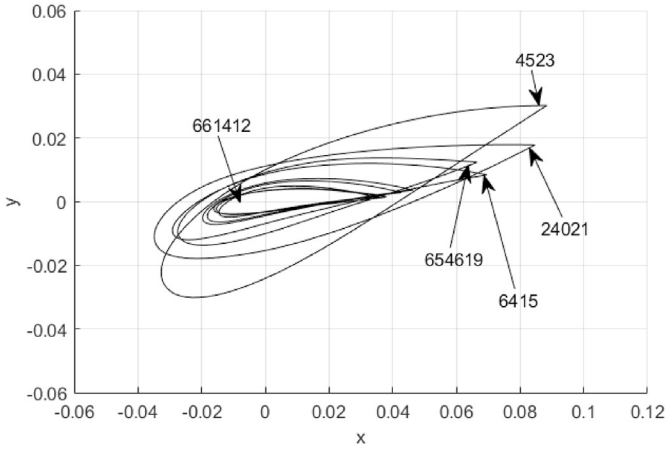

Fig. 8. 2-D section view of blade profile of Selected Solution 2.

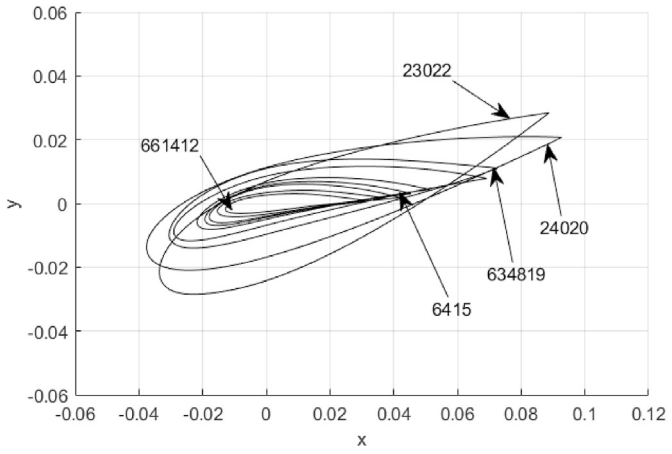

Fig. 9. 2-D section view of blade profile of Selected Solution 3.

Solution 1 at a TSR = 9 and above. The thrust coefficients for both Solution 2 and 3 are lower across the range of TSRs with Solution 2 having the lowest thrust coefficients when compared with the other solutions, which is expected as it has the lowest f_3 value.

The bending moment of the blades at TSRs of 5, 6, and 7 are compared in Fig. 13, which shows that all three solutions have overall lower bending moments at all radial position, except for solution 1 which has a slightly higher bending moment at the blade tip. Solution 2 demonstrates the lowest bending moment across all radial position except for the blade tip where it is slightly higher than Solution 3. It is worth noting that these plots are predicted values using Equation (16) where R = 10 m.

The NSGA-BEM model in the current study outputs a large number of Pareto solutions, with 248 solutions in the Pareto Frontier, which helps narrow down the choices to select a suitable solution out of a total of 30,000 solutions. Each solution in the Pareto Frontier has its own advantages and trade-offs. In this study, Solution 1 demonstrates an overall increase in power coefficients when compared to the sample blade while having an overall slightly lower thrust coefficient. As a result, the tidal current turbine blade experiences overall lower bending moment. Solution 2 and 3, on the other hand, have demonstrated an overall lower thrust coefficient and bending moment but only slightly better in in terms of power coefficients at a TSR of 6 and above.

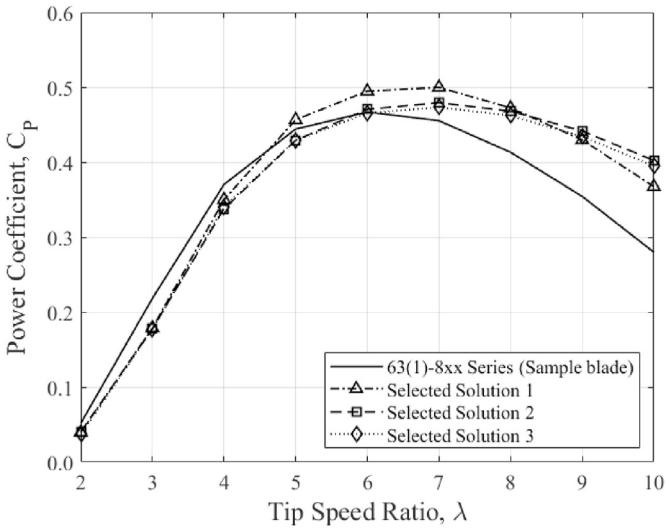

Fig. 11. Power coefficient versus tip speed ratio for the three optimised tidal current turbine blades from E-GABEM (a) and NS-GABEM (b).

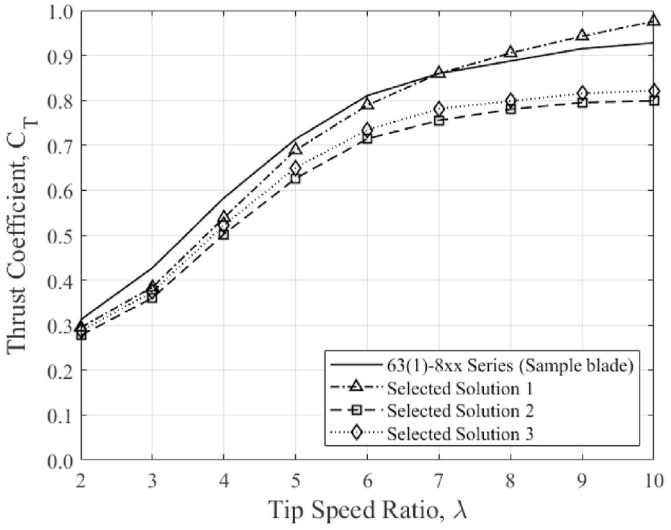

Fig. 12. Thrust coefficient versus tip speed ratio for the three optimised tidal current turbine blades from E-GABEM (a) and NS-GABEM (b).

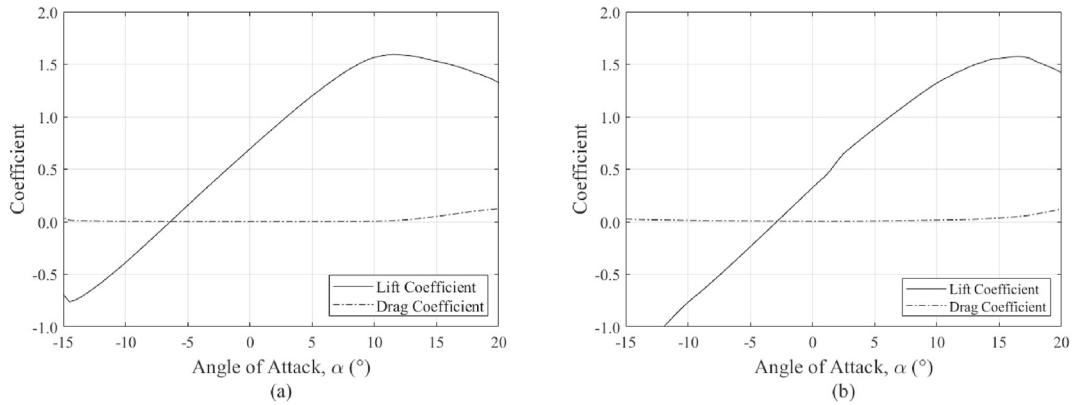

Fig. 10. Lift and drag coefficients of (a) NACA 6415 and (b) 661,412.

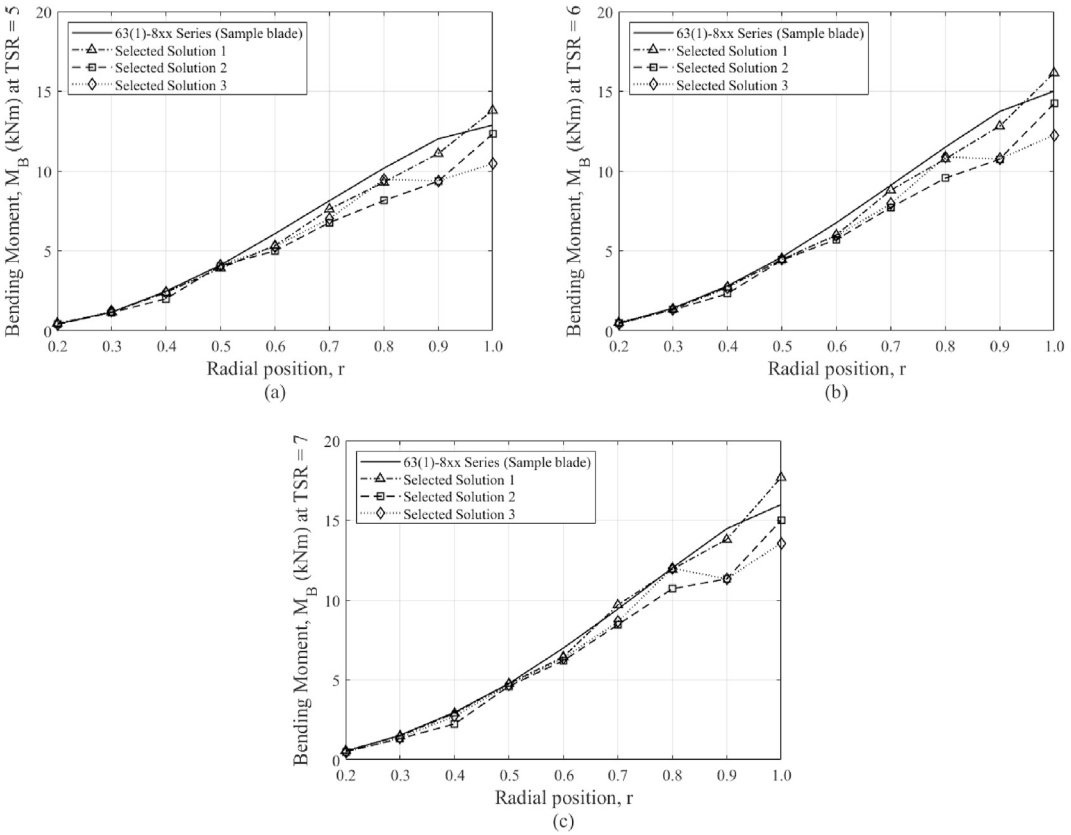

Fig. 13. Comparison of bending moment of at each radial position for (a) TSR = 5, (b) TSR = 6, and (c) TSR = 7.

5. Conclusion

The improved blade element momentum (BEM) theory was validated against an experimentally validated tidal current turbine blade, with coefficient of determination (R^2) values of 0.99828 and 0.99488 for power and thrust coefficients respectively when compared against the measured data. Using XFoil to obtain the lift and drag coefficients of each NACA profile generated, the BEM model in the current study has demonstrated that it is capable of efficiently predicting the hydrodynamic performances of tidal current turbines to a high degree of accuracy.

The work presented in this paper demonstrates a novel approach to combine non-dominated sorting genetic algorithm (NSGA) and the improved BEM model that is capable of accurately capturing the downwash angle, as well as a NACA generator that is capable of reproducing any NACA profile. Such a tool allows the solver to analyse each profile used in each spanwise blade element, producing tidal current turbine blades that have been optimised not only for local twist angle and chord length, but also for suitable NACA profiles to be used at a particular spanwise blade element. The NSGA-BEM model treats each spanwise blade element as a gene and each tidal current turbine (TCT) blade profile as a chromosome, the model has efficiently produced 30,000 TCT blade profiles in approximately 16 hours, 248 of which are in the Pareto Frontier (optimal solutions). Three solutions were manually selected from the Pareto Frontier base on several criteria and compared with measured data from a tidal current turbine blade. The findings have demonstrated an overall improvement in hydrodynamic performances as well as lowering the resulting bending moment experienced by the tidal current turbine blades. Further work will include computational fluid dynamics to extensively study the selected solutions and to validate the results presented in this paper.

Declaration of competing interest

The authors declare that they have no known competing financial interests or personal relationships that could have appeared to influence the work reported in this paper.

References

[1] Taylor Trey. Most marine renewable energy produced in the United States has been in New York city by verdant power – a tidal energy company with global commercial operations underway. VerdantPower; 2021. https://www.verdantpower.com/rite-performance-06-23-21.

[2] Secretariat NWE. Magallanes reinstall ATIR tidal turbine at EMEC. Interreg North-West Europe; 2021. https://www.nweurope.eu/projects/project-search/oceandemo-demonstration-programme-for-ocean-energy-pilot-farms-and-supporting-technologies/news/magallanes-reinstall-atir-tidal-turbine-at-emec/.

[3] SIMEC Atlantis Energy. SAE achieves another tidal milestone – tidal power generation facility in Japan has passed the pre-use inspections test. SIMEC Atlantis Energy Limited; 2021. https://simecatlantis.com/2021/05/24/sae-achieves-another-tidal-milestone-in-japan/#:~:text=SAE is pleased to announce,an official power generation facility.

[4] Zhang L, Wang S, Sheng Q, Jing F, Ma Y. The effects of surge motion of the floating platform on hydrodynamics performance of horizontal-axis tidal current turbine. Renew Energy 2014;74:796–802. https://doi.org/10.1016/j.renene.2014.09.002.

[5] Shi W, Atlar M, Norman R. Detailed flow measurement of the field around tidal turbines with and without biomimetic leading-edge tubercles. Renew Energy 2017;111:688–707. https://doi.org/10.1016/J.RENENE.2017.04.053. Oct.

[6] Liu P, Bose N. Prototyping a series of bi-directional horizontal axis tidal turbines for optimum energy conversion. Appl Energy 2012;99:50–66. https://doi.org/10.1016/J.APENERGY.2012.04.042. Nov.

[7] Liu P, et al. Model testing of a series of bi-directional tidal turbine rotors. Energy 2014;67:397–410. https://doi.org/10.1016/J.ENERGY.2013.12.058.

Apr.
[8] Huang B, Zhu GJ, Kanemoto T. Design and performance enhancement of a bi-directional counter-rotating type horizontal axis tidal turbine. Ocean Eng 2016;128(August):116–23. https://doi.org/10.1016/j.oceaneng.2016.10.012.
[9] Barbarelli S, et al. Design procedure of an innovative turbine with rotors rotating in opposite directions for the exploitation of the tidal currents. Energy 2014;77:254–64. https://doi.org/10.1016/J.ENERGY.2014.08.044. Dec.
[10] Dai JC, Hu YP, Liu DS, Long X. Aerodynamic loads calculation and analysis for large scale wind turbine based on combining BEM modi fied theory with dynamic stall model, vol. 36; 2011. https://doi.org/10.1016/j.renene.2010.08.024.
[11] Hansen MOL, Sørensen JN, Voutsinas S, Sørensen N, Madsen HA. State of the art in wind turbine aerodynamics and aeroelasticity, vol. 42; 2006. p. 285–330. https://doi.org/10.1016/j.paerosci.2006.10.002.
[12] Lanzafame R, Messina MA. Fluid dynamics wind turbine design : critical analysis , optimization and application of BEM theory, vol. 32; 2007. p. 2291–305. https://doi.org/10.1016/j.renene.2006.12.010.
[13] Buhl MLJ. A new empirical relationship between thrust coefficient and induction factor for the turbulent windmill state. National Renewable Energy Laboratory; 2005.
[14] Kavari G, Tahani M, Mirhosseini M. Wind shear effect on aerodynamic performance and energy production of horizontal axis wind turbines with developing blade element momentum theory. J Clean Prod 2019;219:368–76. https://doi.org/10.1016/j.jclepro.2019.02.073.
[15] Abutunis A, Chandrashekhara K. A neural network approach to enhance blade element momentum theory performance for horizontal axis hydrokinetic turbine application, vol. 136; 2019. https://doi.org/10.1016/j.renene.2018.09.105.
[16] Vogel CR, Willden RHJJ, Houlsby GT. Blade element momentum theory for a tidal turbine. Ocean Eng 2018;169(July):215–26. https://doi.org/10.1016/j.oceaneng.2018.09.018.
[17] Masters I, Chapman JC, Willis MR, Orme JAC. A robust blade element momentum theory model for tidal stream turbines including tip and hub loss corrections. J. Mar. Eng. Technol. 2011;10(1):25–35. https://doi.org/10.1080/20464177.2011.11020241.
[18] El-shahat SA, Li G, Lai F, Fu L. Investigation of parameters affecting horizontal axis tidal current turbines modeling by blade element momentum theory. Ocean Eng 2020;202(January):107176. https://doi.org/10.1016/j.oceaneng.2020.107176.
[19] Bahaj AS, Batten WMJ, McCann G. Experimental verifications of numerical predictions for the hydrodynamic performance of horizontal axis marine current turbines. Renew Energy 2007;32(15):2479–90. https://doi.org/10.1016/J.RENENE.2007.10.001. Dec.
[20] Selig MS, Coverstone-Caroll VL. Application of a genetic algorithm to wind turbine design. J Energy Resour Technol 1996;118(1):22–8. https://doi.org/10.1115/1.2792688.
[21] Sessarego M, Dixon KR, Rival DE, Wood DH. A hybrid multi-objective evolutionary algorithm for wind-turbine blade optimization, vol. 273; 2015. https://doi.org/10.1080/0305215X.2014.941532.
[22] Hu W, Park D, Choi D. Stuctural optimization procedure of a composite wind turbine blade for reducing both material cost and blade weight. Eng Optim 2013;45(12):1469–87. https://doi.org/10.1080/0305215X.2012.743533.
[23] Mortazavi SM, Soltani MR, Motieyan H. A Pareto optimal multi-objective optimization for a horizontal axis wind turbine blade airfoil sections utilizing exergy analysis and neural networks. Inl. Wind Eng. Ind. Aerodyn. 2015;136:62–72. https://doi.org/10.1016/j.jweia.2014.10.009.
[24] Gentils T, Wang L, Kolios A. Integrated structural optimisation of offshore wind turbine support structures based on finite element analysis and genetic algorithm. Appl Energy 2017;199:187–204. https://doi.org/10.1016/j.apenergy.2017.05.009.
[25] Abdelsalam AM, El-shorbagy MA. Optimization of wind turbines siting in a wind farm using genetic algorithm based local search. Renew Energy 2018;123:748–55. https://doi.org/10.1016/j.renene.2018.02.083.
[26] Sun H, Qiu C, Lu L, Gao X, Chen J, Yang H. Wind turbine power modelling and optimization using artificial neural network with wind field experimental data. Appl Energy 2020;280(July):115880. https://doi.org/10.1016/j.apenergy.2020.115880.
[27] Yang Q, Hu J, Law S. Journal of Wind Engineering & Industrial Aerodynamics Optimization of wind farm layout with modi fi ed genetic algorithm based on boolean code. J Wind Eng Ind Aerod 2018;181(September):61–8. https://doi.org/10.1016/j.jweia.2018.07.019.
[28] Neto JXV, Guerra Junior EJ, Moreno SR, Ayala HVH, Mariani VC, dos Santos Coelho L. Wind turbine blade geometry design based on multi-objective optimization using metaheuristics, vol. 162; 2019. p. 645–58. https://doi.org/10.1016/j.energy.2018.07.186. 2018.
[29] Benini E, Toffolo A. Optimal design of horizontal-Axis wind turbines using blade-element theory and evolutionary computation. J Sol Energy Eng 2002;124(4):357–63. https://doi.org/10.1115/1.1510868.
[30] Mellal MA, Pecht M. A multi-objective design optimization framework for wind turbines under altitude consideration. Energy Convers Manag 2020;222(July):113212. https://doi.org/10.1016/j.enconman.2020.113212.
[31] Civelek Z. Optimization of fuzzy logic (Takagi-Sugeno) blade pitch angle controller in wind turbines by genetic algorithm. Eng. Sci. Technol. an Int. J. 2020;23(1):1–9. https://doi.org/10.1016/j.jestch.2019.04.010.
[32] Sale D. Hydrodynamic optimization method and design code for stall-regulated hydrokinetic turbine rotors. 2009. August.
[33] Kolekar N, Banerjee A. Performance characterization and placement of a marine hydrokinetic turbine in a tidal channel under boundary proximity and blockage effects. Appl Energy 2015;148:121–33. https://doi.org/10.1016/j.apenergy.2015.03.052.
[34] Zhu F, Ding L, Huang B, Bao M, Liu J. Blade design and optimization of a horizontal axis tidal turbine. Ocean Eng 2020;195:106652. https://doi.org/10.1016/j.oceaneng.2019.106652.
[35] Menéndez Arán D, Menéndez Á. Surrogate-based optimization of horizontal axis hydrokinetic turbine rotor blades. Energies 2021;14(13). https://doi.org/10.3390/en14134045.
[36] Coiro DP, Daniele E, Della Vecchia P. Diffuser shape of optimization for GEM, a tethered system based on two horizontal axis hydro turbines. 2014. https://doi.org/10.13140/2.1.4194.1125.
[37] Lo Brutto OA, Thiébot J, Guillou SS, Gualous H. A semi-analytic method to optimize tidal farm layouts – application to the Alderney Race (Raz Blanchard), France. Appl Energy 2016;183:1168–80. https://doi.org/10.1016/j.apenergy.2016.09.059.
[38] Nandagopal RA, Narasimalu S. Multi-objective optimization of hydrofoil geometry used in horizontal axis tidal turbine blade designed for operation in tropical conditions of South East Asia. Renew Energy 2020;146:166–80. https://doi.org/10.1016/j.renene.2019.05.111.
[39] Tahani M, Babayan N, Razi F, Moghadam A. Multi objective optimization of horizontal axis tidal current turbines , using Meta heuristics algorithms. Energy Convers Manag 2015;103:487–98. https://doi.org/10.1016/j.enconman.2015.06.086.
[40] Thandayutham K, Avital EJ. Optimization of a horizontal axis marine current turbine via surrogate models. 2019. https://doi.org/10.12989/ose.2019.9.2.111. May.
[41] Seo J, Yi J, Park J, Lee K. Review of tidal characteristics of Uldolmok Strait and optimal design of blade shape for horizontal axis tidal current turbines. Renew Sustain Energy Rev 2019;113(May):109273. https://doi.org/10.1016/j.rser.2019.109273.
[42] Zhu J, Cai X, Gu R. Multi-objective aerodynamic and structural optimization of horizontal-axis wind turbine blades. Energies 2017. https://doi.org/10.3390/en10010101.
[43] Yeo EJ, Kdenneedly DM, O'Rourke F. Tidal current turbine blade optimisation using a combined non-dominated sorting genetic algorithm – blade element momentum theory. In: Proc. Eur. Wave tidal energy conf.; 2021. 2209-1–2209–10. April 2017.
[44] Glauert H. The analysis of experimental results in the windmill brake and vortex ring states of an airscrew. 1926. ARCR R&M No. 1026.
[45] Wilson RE, L. P.B.S.. Applied aerodynamics of wind power machines. *Natl. Sci. Found.*, no. Oregon State University; 1974.
[46] Wilson RE, Lissaman PBS, Walker SN. Aerodynamic performance of wind turbines. Natl. Sci. Found.; 1976. ERDA/NSF/04014-76/1.
[47] Wood DH, Okulov VL. Nonlinear blade element-momentum analysis of Betz-Goldstein rotors. Renew Energy 2017;107:542–9. https://doi.org/10.1016/j.renene.2017.02.027.
[48] Shen WZ, Mikkelsen R, Sørensen JN, Bak C. Tip loss corrections for wind turbine computations. Wind Energy 2005;8(4):457–75.
[49] W. Zhong, W. Z. Shen, T. Wang, and Y. Li, "A tip loss correction model for wind turbine aerodynamic performance prediction," Renew Energy, vol. 147, pp. 223–238, Mar. 2020, doi: 10.1016/j.renene.2019.08.125.
[50] Kolekar N, Banerjee A. A coupled hydro-structural design optimization for hydrokinetic turbines. J Renew Sustain Energy 2013;5(5):1–22. https://doi.org/10.1063/1.4826882.
[51] Van Treuren KW. Small-Scale wind turbine testing in wind tunnels under low Reynolds number conditions. J Energy Resour Technol 2015;137(5):51208. https://doi.org/10.1115/1.4030617.
[52] Mack S, Brehm C, Heine B, Kurz A, Fasel H. Experimental investigation of separation and separation control on a laminar airfoil. 2008. https://doi.org/10.2514/6.2008-3766.
[53] Timmer WA, Bak C. 4 - aerodynamic characteristics of wind turbine blade airfoils. In: Brøndsted P, Nijssen RPL, editors. Advances in wind turbine blade design and materials. Woodhead Publishing; 2013. p. 109–49.
[54] Zhu WJ, Shen WZ, Sørensen JN. Integrated airfoil and blade design method for large wind turbines. Renew Energy 2014;70:172–83. https://doi.org/10.1016/j.renene.2014.02.057.
[55] Pires O, Munduate X, Ceyhan O, Jacobs M, Snel H. Analysis of high Reynolds numbers effects on a wind turbine airfoil using 2D wind tunnel test data Analysis of high Reynolds numbers effects on a wind turbine airfoil using 2D wind tunnel test data. J. Phys. Conf. Ser. 2016;753(2). https://doi.org/10.1088/1742-6596/753/2/022047.
[56] Pires O, Munduate X, Ceyhan O, Jacobs M, Madsen J, Schepers JG. Analysis of the high Reynolds number 2D tests on a wind turbine airfoil performed at two different wind tunnels Analysis of the high Reynolds number 2D tests on a wind turbine airfoil performed at two different wind tunnels. In: WindEurope summit 2016 27-29 september 2016, vol. 749; 2016. https://doi.org/10.1088/1742-6596/749/1/012014. no. 2.
[57] Selig MS. Low Reynolds number airfoil design lecture notes. von Karman Institute for Fluid Dynamics or NATO-RTO/AVT; 2003.
[58] Morgado J, Vizinho R, Silvestre MAR, Páscoa JC. XFOIL vs CFD performance predictions for high lift low Reynolds number airfoils. Aero Sci Technol 2016;52:207–14. https://doi.org/10.1016/j.ast.2016.02.031.

[59] Ouro P, Harrold M, Stoesser T, Bromley P. Hydrodynamic loadings on a horizontal axis tidal turbine prototype. J Fluid Struct 2017;71:78–95. https://doi.org/10.1016/j.jfluidstructs.2017.03.009.
[60] Goldberg DE, Holland JH. Genetic algorithms and machine learning. The Netherlands: Kluwer Academic Publishers; 1988.
[61] Schmitt LM. Theory of genetic algorithms. Theor Comput Sci 2001;259:1–61. https://doi.org/10.1016/S0304-3975(00)00406-0.
[62] Wang R. An Improved Nondominated Sorting Genetic Algorithm for Multi-objective Problem, 2016; 2016.
[63] Elarbi M, Bechikh S, Gupta A, Ben Said L, Ong Y. A new decomposition-based NSGA-II for many-objective optimization, vol. 48; 2018. p. 1191–210. 7.
[64] Bahaj AS, Molland AF, Chaplin JR, Batten WMJ. Power and thrust measurements of marine current turbines under various hydrodynamic flow conditions in a cavitation tunnel and a towing tank, vol. 32; 2007. p. 407–26. https://doi.org/10.1016/j.renene.2006.01.012.
[65] A. de Haro, "NACA airfoil generator," Github. https://github.com/adeharo9/NACA-airfoil-generator.